Dynamic flow resistivity based model for sound absorption of multi-layer sintered fibrous metals

MENG Han[1], AO QingBo[2], TANG HuiPing[2], XIN FengXian[1*] & LU TianJian[1]

[1] *State Key Laboratory for Mechanical Structure Strength and Vibration, School of Aerospace, Xi'an Jiaotong University, Xi'an 710049, China;*
[2] *State Key Laboratory of Porous Metal Materials, Northwest Institute for Nonferrous Metal Research, Xi'an 710016, China*

The sound absorbing performance of the sintered fibrous metallic materials is investigated by employing a dynamic flow resistivity based model, in which the porous material is modeled as randomly distributed parallel fibers specified by two basic physical parameters: fiber diameter and porosity. A self-consistent Brinkman approach is applied to the calculation of the dynamic resistivity of flow perpendicular to the cylindrical fibers. Based on the solved flow resistivity, the sound absorption of single layer fibrous material can be obtained by adopting the available empirical equations. Moreover, the recursion formulas of surface impedance are applied to the calculation of the sound absorption coefficient of multi-layer fibrous materials. Experimental measurements are conducted to validate the proposed model, with good agreement achieved between model predictions and tested data. Numerical calculations with the proposed model are subsequently performed to quantify the influences of fiber diameter, porosity and backed air gap on sound absorption of uniform (single-layer) fibrous materials. Results show that the sound absorption increases with porosity at higher frequencies but decreases with porosity at lower frequencies. The sound absorption also decreases with fiber diameter at higher frequencies but increases at lower frequencies. The sound absorption resonance is shifted to lower frequencies with air gap. For multi-layer fibrous materials, gradient distributions of both fiber diameter and porosity are introduced and their effects on sound absorption are assessed. It is found that increasing the porosity and fiber diameter variation improves sound absorption in the low frequency range. The model provides the possibility to tailor the sound absorption capability of the sintered fibrous materials by optimizing the gradient distributions of key physical parameters.

1   Introduction

Sintered fibrous materials are typically fabricated with micron-sized metallic fibers (e.g., stainless steel and FeCrAl) through the processes of non-woven lay, superposition, and sintering at high temperature. The as-fabricated material has high porosity (more than 90%) and complicated tortuosity amongst micron-sized fibers (see Figure 1), resulting in superior sound absorption performance due mainly to viscous damping and thermal loss. Apart from the sound absorption ability, the sintered fibrous material also has attractive mechanical properties, and hence may be exploited for noise control applications under extreme circumstances, e.g., acoustical liner of turbofan engine inlet [1–3].

The sound absorption properties of uniform (homogeneous) porous materials have been extensively investigated by using phenomenological models that involve a number of parameters, whose values are sometimes difficult to determine. For instance, Zwikker and Kosten [4] proposed a model to calculate the complex density and bulk modulus of

*Corresponding author (email: fengxian.xin@gmail.com)

rigid frame porous materials, in which the micro-pores were modeled as circular ones. Biot [5,6] developed a phenomenological theory for wave propagating in fluid saturated porous solid, in which the material was represented by four non-dimensional parameters and characteristic frequency. Attenborough [7] presented a theoretical model to estimate the acoustical properties of rigid fibrous absorbent soils and sands, which needs five parameters including porosity, flow resistivity, tortuosity, steady flow shape factor and dynamic shape factor. Attenborough's model could only give good predictions for soils and sands with high flow resistivity especially at low frequencies. Johnson et al. [8] constructed an analytical model to evaluate the dynamic tortuosity of fluid-saturated porous media. Based upon Johnson et al.'s model, Champoux and Allard [9] proposed formulae to calculate the dynamic bulk modulus of air-saturated porous media by introducing the concept of characteristic length. By approximating the relaxation characteristic, Wilson [10] developed a model for the complex density and bulk modulus of a porous medium without using any Bessel functions. Being built upon the dynamic density of Biot and the dynamic bulk modulus of Zwikker and Kosten, the so-called Biot-Allard model was formulated for porous materials [11]. Recently, Zhang and Chen [2] used the extended Biot-Allard model to calculate the sound absorption characteristics of porous sintered fiber metals. A number of parameters including shape factor, sinuosity and flow resistivity were needed to complete the calculation. However, as the Biot-Allard model is more suitable for porous media having single pore size scale [10], it is not capable of accounting for the fractal surface and complicated topologies of the sintered fiber metals (Figure 1).

Apart from phenomenological models, a number of empirical models were also established. Narang [12] proposed an empirical model to predict the flow resistivity of polyester fibrous materials in terms of the number of fibers per volume. The characteristic impedances of several porous materials including elastic, rigid-frame and fibrous porous materials as well as loose granular media were empirically estimated by Voronina [13–17]. On the basis of a series of
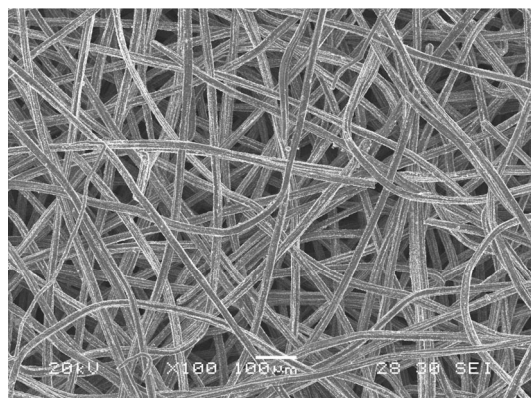

Figure 1 Typical topology of the sintered fibrous metal.

experimental measurements, Garai and Pompoli [18] developed an empirical model to estimate the flow resistivity, acoustic impedance and sound absorption coefficient of polyester fibrous materials. Whilst the empirical models as mentioned above may give accurate predictions in specific cases, they do not possess generality of being suitable for every common porous material. The most popular and widely used empirical model was proposed by Delany and Bazley [19], in which simple power-law functions for characteristic impedance and propagation constant were formulated on the basis of experimental data. As a modification, Miki [20] gave new expressions for acoustic impedance and propagation constant based on Delany and Bazley's experimental data. Instead of the phenomenological equations of Delany and Bazley, Allard and Champoux [21] derived new expressions by using the general frequency dependence of viscous forces in porous materials [8]. Further, Komatsu [22] improved the two conventional models, i.e., the Deleny-Bazley model and the Miki model, to give more accurate predictions for high-density fibrous materials as well as low-density ones.

Although the sintered fibrous metals have excellent sound absorption properties [1–3], there is still room for improvement especially in low frequency range where their sound absorption capability is relatively poor. The most obvious and effective way is to optimize the key topological parameters influencing sound propagating in the fibrous material. For instance, it has been suggested that introducing gradients of certain parameters can improve the sound absorption performance of porous materials [23–25]. However, a feasible theoretical model is needed to qualify the gradient optimization framework and predict optimal gradient parameter distributions. This deficiency is addressed in the present study.

A theoretical model based on dynamic flow resistivity is proposed to characterize the sound absorption properties of (both uniform and multi-layer) sintered fibrous materials, involving only two topological parameters (i.e., fiber diameter and porosity). The porous material is modeled as randomly distributed parallel fibers so that the dynamic flow resistivity can be favorably estimated by using Tarnow's method [26]. The sound absorption coefficient of the fibrous material is then obtained on the basis of the propagation constant and characteristic impedance (expressed in terms of dynamic flow resistivity). Applying the recursion formulae for surface impedance enables calculating the sound absorption coefficient of multi-layer fibrous material. The model is validated against experimental measurements for both uniform fibrous materials and multi-layer ones.

2 Theory

As shown in Figure 1, the sintered fibrous material is composed of twisted metal fibers connected by the sintered

points between the fibers. Since the fibers generally lie in planes parallel to the surface of fibrous metal sheet, the fibrous materials may be regarded as transverse isotropic. When sound is normally incident on the fibrous metal sheet, the resisting force for sound propagation is mainly caused by the fibers. For simplicity, contribution of the sintered points to the resistance is ignored as they occupy much less surface area in comparison with the fibers. Further, the length of the fiber between two connecting sintered points is taken to be sufficiently large relative to its diameter. Although the factual fibers are distributed randomly with the sintered points, their fluid resistivity may be evaluated approximately from a stack of randomly distributed parallel circular fibers having the same porosity as that of the randomly distributed fibers, as shown in Figure 2. Note that for the sintered fibrous metal, the density and stiffness of the fibers are much larger than those of the air in the fibrous material, the fibers can be treated as motionless fibers when the sound is propagated through the fibrous material.

A self-consistent Brinkman approach is employed to calculate the dynamic resistivity of flow perpendicular to the cylindrical fibers. Only one fiber placed at the center of the coordinate system is considered as shown in Figure 3. The influence of all the other cylinders on this one is accounted for by introducing a body force $-R'_\perp \boldsymbol{u}$ into the Navier-Stokes equation, as [26]

$$-\mathrm{j}\omega\rho_0\boldsymbol{u} = -\nabla p + \eta\nabla^2\boldsymbol{u} - R'_\perp\boldsymbol{u}, \tag{1}$$

where ω is angular frequency, ρ_0 is the density of air, $\boldsymbol{u}$ is the velocity vector, p is the pressure around the fiber and η is the viscosity of air. The symbol $R'_\perp$ is the factor proportionality to the velocity of the body force.

To solve the equation, two boundary conditions are applied:
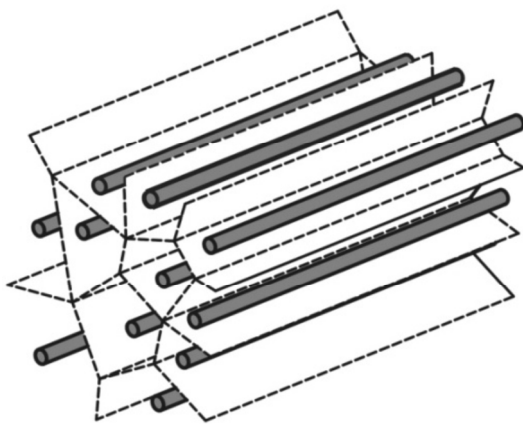
$$\boldsymbol{u}(a) = 0, \tag{2}$$

Figure 2　Parallel cylindrical fibers with surrounding Voronoi polygons, the latter constructed by perpendicular bisectors of connecting line between every two cylinder circle centers.
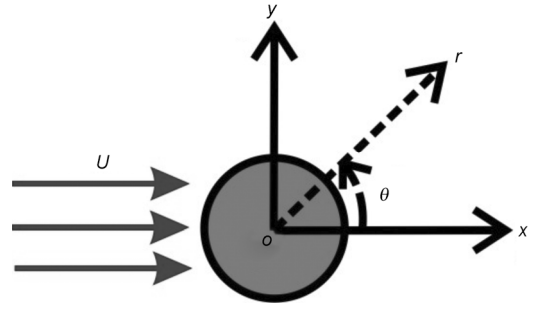
Figure 3　Schematic of one fiber for the theoretical formulation.

$$\boldsymbol{u}(\infty) = (U, 0, 0), \tag{3}$$

where a is the radius of the fibers and U is the mean velocity of the flow (Figure 2).

A solution to eq. (1) subjected to the boundary conditions of eqs. (2) and (3) may be expressed in terms of Hankel function as:

$$u_r = \left(U - \frac{b_1}{r^2} + \frac{1}{r}H_1^1(k'_\perp r)\right)\cos\theta, \tag{4}$$

$$u_\theta = -\left(U + \frac{b_1}{r^2} + hk'_\perp H_1^{1'}(k'_\perp r)\right)\sin\theta, \tag{5}$$

where $H_1^1(\cdot)$ represents the first order Hankel function of the first kind, the prime on the Hankel function indicates the derivative, $k'_\perp$, h and b_1 are constants given by:

$$k'_\perp = \sqrt{\frac{\mathrm{j}\omega\rho_0 - R'_\perp}{\eta}}, \tag{6}$$

$$h = -\frac{2U}{k'_\perp H_0^1(k'_\perp a)}, \tag{7}$$

$$b_1 = a^2\left(1 - \frac{2H_1^1(k'_\perp a)}{k'_\perp a H_0^1(k'_\perp a)}\right)U. \tag{8}$$

Therefore, the viscous drag force per length on the cylinder may be calculated in terms of pressure and the stress tensor, as [26]

$$F_\perp = 2\pi\eta U k'_\perp a\left(-k'_\perp a + \frac{2H_1^1(k'_\perp a)}{H_0^1(k'_\perp a)}\right). \tag{9}$$

Besides, the introduced body force per volume should equal the viscous drag force on the cylinder per volume:

$$R'_\perp U = F_\perp / b^2, \tag{10}$$

where b^2 is the mean area of the Voronoi cells surrounding the fibers, which is related to the porosity of the fibrous material as:

$$\Omega = \frac{b^2 - \pi a^2}{b^2}. \tag{11}$$

Thus, the factor proportionality to the velocity of the introduced body force is

$$R'_\perp = \frac{2\pi\eta k'_\perp a}{b^2}\left(-k'_\perp a + \frac{2H_1^1(k'_\perp a)}{H_0^1(k'_\perp a)}\right). \tag{12}$$

A simple self-iterative calculation of Brinkman [27] is applied to solve eqs. (6) and (12). The resistivity $R'_\perp$ is firstly calculated from eq. (12) by postulating $k'_\perp$ having a certain value, for example $k'_\perp = j/b$. A new $k'_\perp$ is then computed from eq. (6) afterwards, the new $k'_\perp$ is substituted into eq. (12) again. The preceding processes are repeated until stable values of $k'_\perp$ and $R'_\perp$ are obtained.

Finally, with the inertia of air between the cylinders considered, the dynamic resistivity for flow perpendicular to the random cylinders (i.e., the fibrous material) is obtained as

$$R_\perp = -j\omega\rho_0 + R'_\perp. \tag{13}$$

The dynamic resistivity is then applied to predict the propagation constant and characteristic impedance of the fibrous material using the empirical formulas proposed by Komatsu [22]. Even though the static resistivity is used in Komatsu's model, the application of the dynamic resistivity changing with frequency is expected to present more accurate predictions. The propagation constant Γ is

$$\Gamma = \alpha + i\beta, \tag{14}$$

$$\alpha = 0.0069\frac{\omega}{c_0}\left(2 - \log\frac{f}{R_\perp}\right)^{4.1}, \tag{15}$$

$$\beta = \frac{\omega}{c_0}\left[1 + 0.0004\left(2 - \log\frac{f}{R_\perp}\right)^{6.2}\right], \tag{16}$$

where c_0 is sound speed in air and f is the frequency.

The characteristic impedance Z is given by

$$Z = \varsigma + i\xi, \tag{17}$$

$$\varsigma = \rho_0 c_0\left[1 + 0.00027\left(2 - \log\frac{f}{R_\perp}\right)^{6.2}\right], \tag{18}$$

$$\xi = -\rho_0 c_0\left[0.0047\left(2 - \log\frac{f}{R_\perp}\right)^{4.1}\right]. \tag{19}$$

For fibrous material backed by an impervious rigid wall, the surface impedance may be calculated from its characteristic impedance, as

$$Z_s(\omega) = Z(\omega)\coth[\Gamma(\omega)h], \tag{20}$$

where h is the thickness of the fibrous material sample.

Eventually, the sound absorption coefficient α of the fibrous material sample is obtained as

$$\alpha = 1 - \left|\frac{Z_s - \rho_0 c_0}{Z_s + \rho_0 c_0}\right|^2. \tag{21}$$

Consider next a multi-layer fibrous material sample that is composed of several layers of different fibrous materials as shown schematically in Figure 4. The calculation of its surface impedance is similar to but more complex than that of a single-layer one. Assuming a plane sound wave passing through the $(n-1)$th layer of the multi-layer sample as shown in Figure 4, one may express the sound pressure in the nth layer as

$$p = P_i e^{j(\omega t - k_{n-1}x)} + P_r e^{j(\omega t + k_{n-1}x)}, \tag{22}$$

where P_i, P_r are the amplitudes of the incident and reflected waves, respectively, $k_{n-1} = \Gamma_{n-1}/j$ is the wavenumber in the $(n-1)$th layer (between x_n and x_{n-1}), which also has the relationship with sound speed c_{n-1} in the $(n-1)$th layer as

$$k_{n-1} = \omega/c_{n-1}. \tag{23}$$

The sound velocity of the fibrous material is then calculated by the sound pressure, as

$$v = \frac{-1}{j\omega\rho_{n-1}}\frac{\partial p}{\partial x} = \frac{k_{n-1}}{\omega\rho_{n-1}}\left(P_i e^{j(\omega t - k_{n-1}x)} - P_r e^{j(\omega t + k_{n-1}x)}\right), \tag{24}$$

where ρ_{n-1} is the density of the fibrous material in the $(n-1)$th layer.

The surface impedance $Z_s(x_{n-1})$ may be calculated as

$$Z_s(x_{n-1}) = \frac{p(x_{n-1})}{v(x_{n-1})} = \rho_{n-1}c_{n-1}\frac{P_i e^{-jk_{n-1}x_{n-1}} + P_r e^{jk_{n-1}x_{n-1}}}{P_i e^{-jk_{n-1}x_{n-1}} - P_r e^{jk_{n-1}x_{n-1}}}. \tag{25}$$

Similarly, the surface impedance $Z_s(x_n)$ is given by

$$Z_s(x_n) = \frac{p(x_n)}{v(x_n)} = \rho_{n-1}c_{n-1}\frac{P_i e^{-jk_{n-1}x_n} + P_r e^{jk_{n-1}x_n}}{P_i e^{-jk_{n-1}x_n} - P_r e^{jk_{n-1}x_n}}, \tag{26}$$
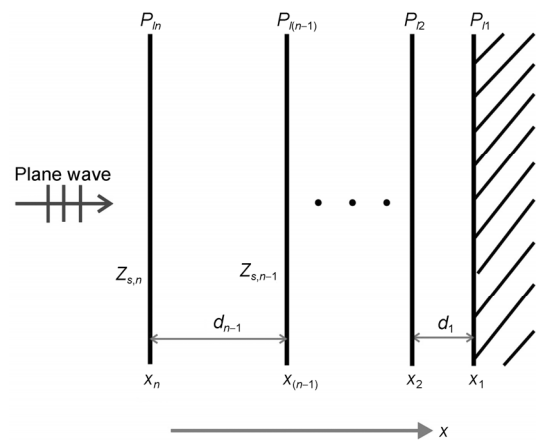

Figure 4 Schematic of sound incident on a multi-layer fibrous material backed by an impervious rigid wall.

It follows from eq. (25) that

$$\frac{P_i}{P_r} = \frac{Z_s(x_{n-1}) + \rho_{n-1}c_{n-1}}{Z_s(x_{n-1}) - \rho_{n-1}c_{n-1}} e^{2jk_{n-1}x_{n-1}}. \qquad (27)$$

Substitution of eq. (27) into eq. (25) leads to

$$Z_s(x_n) = Z_{n-1}\frac{Z_s(x_{n-1})\coth(\Gamma_{n-1}d_{n-1}) + Z_{n-1}}{Z_s(x_{n-1}) + Z_{n-1}\coth(\Gamma_{n-1}d_{n-1})}, \qquad (28)$$

where for the ($n-1$)th layer, $Z_{n-1} = \rho_{n-1}c_{n-1}$ is the characteristic impedance, $d_{n-1} = x_{n-1} - x_n$ is the thickness, and $\Gamma_{n-1} = jk_{n-1}$ is the propagation constant.

It should be mentioned that the recursion formula for surface impedance is suitable for all kinds of multi-layer samples, even for one or more layers being air gap.

3   Comparison between theory and experiment

In this section, the proposed theoretical model for multi-layer fibrous materials is validated against experimental results. The mechanism of sound absorption of randomly distributed parallel fibers is the same as the real fibrous materials, although its pore structure and channel are indeed different from the real material. Both the theoretical and experimental results prove that the randomly distributed parallel fibers can well approximately mimic the real fibrous materials when they have the same geometrical parameters. The tested samples are made of FeCrAl fibers with the same diameter and the length of 10–80 mm, which are randomly distributed and then sintered in a vacuum sintering furnace as a whole. The multi-layer fibrous metals are sintered by several fiber metal felts, which consist of various FeCrAl fibers with different geometrical parameters. Four fibrous metal samples are manufactured with the physical parameters listed in Table 1 for single-layer material and Table 2 for multi-layer material. The fiber diameters of the samples are selected before the preparation, and the porosity can be obtained since the density of the samples and the fibers can be easily tested. The sound absorption coefficient is measured in the B&K 4206 impedance tube in the frequency of 50–6400 Hz with the transfer function method.

The model predictions and experimental measurements are compared in Figures 5 and 6 for single- and multi-layer

fibrous materials, respectively. It can be seen that the theoretical model provides reasonable predictions for sound absorption coefficient of fibrous materials as the predictions match well with the measurements even for the complicated multi-layer cases (Figure 6). The small deviations between the predictions and measurements may be attributed to the simplified handling of the connections between layers in the theory and the inevitable micro-defects of the test samples.

4   Influence of physical parameters: Single-layer fibrous metal

Relevant physical parameters that may affect the sound absorption performance of single-layer fibrous metal samples are listed in Table 3. The theoretical model established in the previous sections is employed to quantify the effects of these parameters upon the sound absorption coefficient of the fibrous materials and explore the mechanisms underlying the associated phenomena.

4.1   Influence of porosity

The predicted influence of porosity on flow resistivity and sound absorption of single-layer fibrous metal sheets having different thicknesses (Table 3) are presented in Figures 7 and 8 respectively. The metal sheets are considered to be in contact with the backing rigid wall with the fixed fiber diameter of 100 μm. It can be seen from Figure 7 that the absolute values of the real and imaginary parts of the flow resistivity both decrease with the increase of the porosity. It can be seen from Figure 8 that the porosity has a significant influence on sound absorption of the fibrous material. As the porosity is increased, the sound absorption coefficient decreases at relatively low frequencies but increases at higher frequencies. Further, irrespective of porosity level, the sound absorption coefficient increases monotonically with increasing frequency until reaching a stable value in the high frequency range. This is mainly because the fibrous

Table 1   Single-layer fibrous material samples

Sample number	Fiber diameter (μm)	Porosity (%)	Thickness (mm)
1	50	91	25
2	50	73	10

Table 2   Multi-layer fibrous material samples

Sample number	Fiber diameter (μm)			Porosity (%)			Thickness (mm)		
	First layer	Second layer	Third layer	First layer	Second layer	Third layer	First layer	Second layer	Third layer
3	100	50	-	77	73	-	10	10	-
4	100	50	25	77	73	73	10	10	10

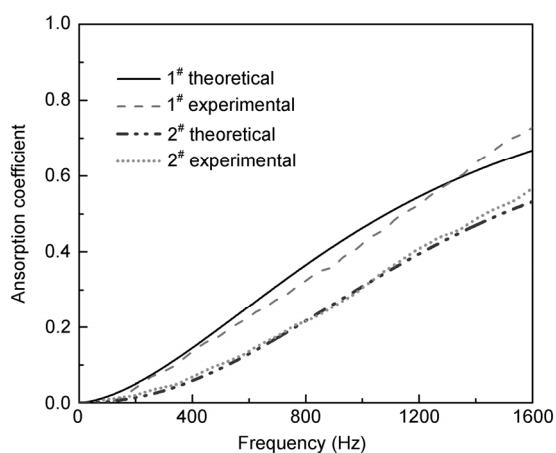The first layer is the layer close to sound resource.

Figure 5 Sound absorption coefficient of uniform fibrous material plotted as a function of frequency: Comparison between model predictions and experimental measurements for samples 1# and 2#.
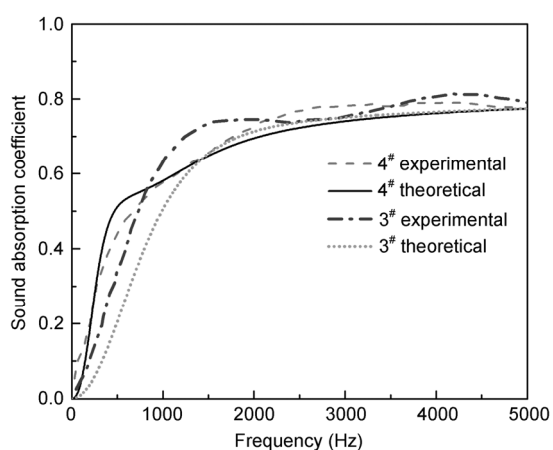

Figure 6 Sound absorption coefficient of multi-layer fibrous material plotted as a function of frequency: Comparison between model predictions and experimental measurements for samples 3# and 4#.

material has superior energy dissipation ability for high frequency sound waves, which reaches a stable state when this ability approaches its extreme value. Note that the
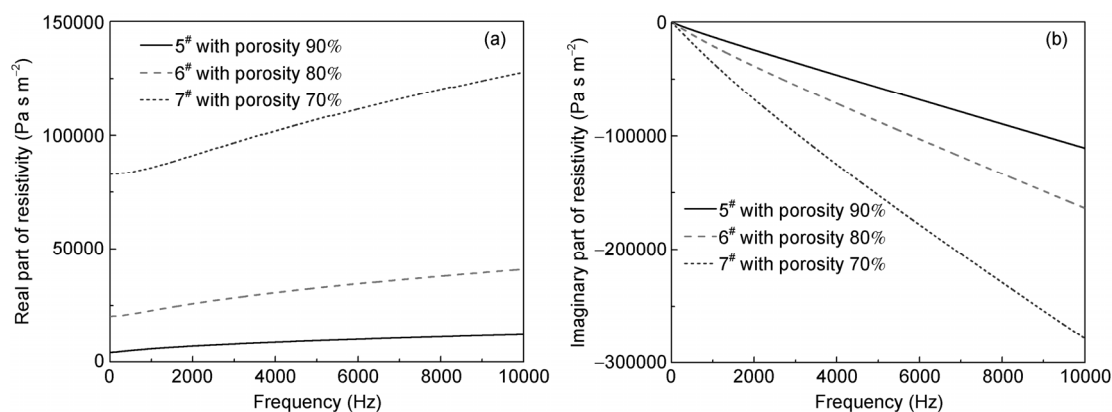
Table 3 Single-layer fibrous metal samples used for physical parameter study

Sample number	Fiber diameter (μm)	Porosity (%)	Thickness (mm)
5	100	90	10
6	100	80	10
7	100	70	10
8	100	90	50
9	100	80	50
10	100	70	50
11	100	95	10
12	50	95	10
13	25	95	10
14	100	95	50
15	50	95	50
16	25	95	50
17	20	95	20
18	50	90	20
19	40	90	20

porosity of the fibrous material dictates how close its characteristic impedance is to that of air. Consequently, it determines the amount of sound entering the porous material and hence affects strongly the maximum stable value of the sound absorption coefficient. In general, the maximum stable value is not equal to unity, because part of the sound energy is reflected at the interface when the characteristic impedance of the fibrous material is not equal to that of air. Note also that the maximum stable value is shifted to lower frequency as the sample thickness is increased, as the increase of sample thickness enhances the sound absorption ability of the fibrous material in the low frequency range.

4.2 Influence of fiber diameter

For single-layer fibrous metal sheets having different thicknesses (Table 3), Figures 9 and 10 present the influence of fiber diameter on the flow resistivity and sound absorption of the material. The metal sheets are considered to be in
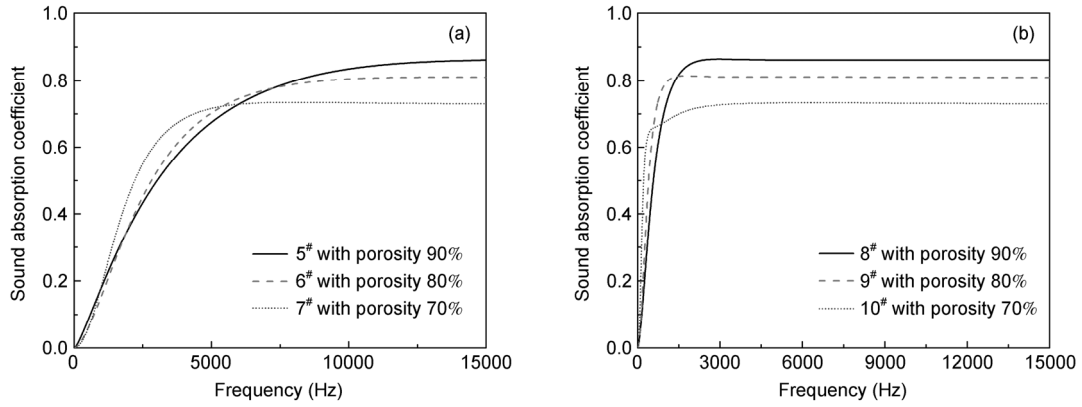

Figure 7 Influence of porosity on flow resistivity of single-layer fibrous metal (samples 5#, 6# and 7#). (a) The real part of flow resistivity; (b) the imaginary part of flow resistivity.

Figure 8   Influence of porosity on sound absorption coefficient of single layer fibrous metal with thickness: (a) 10 mm (samples 5[#], 6[#] and 7[#]); (b) 50 mm (samples 8[#], 9[#] and 10[#]). Fiber diameter fixed at 100 μm; no air cavity between sample and rigid wall.

contact with the backing rigid wall with fixed porosity of 0.95. Figure 9 shows that the absolute values of real and imaginary parts of the flow resistivity increase with decreasing fiber diameter. Figure 10 shows that the sound absorption coefficient is affected by fiber diameter to some extent. In the high frequency range, the sound absorption coefficient increases as the fiber diameter is decreased. This

is because the contact area between the fiber and surrounding air increases with decreasing fiber diameter, increasing the flow resistivity and hence the sound absorption capability of the fibrous material. In contrast, decreasing fiber diameter results in inferior sound absorption in the low frequency range, because the loss of sound energy due to thermal effects may be reduced in this frequency range. As
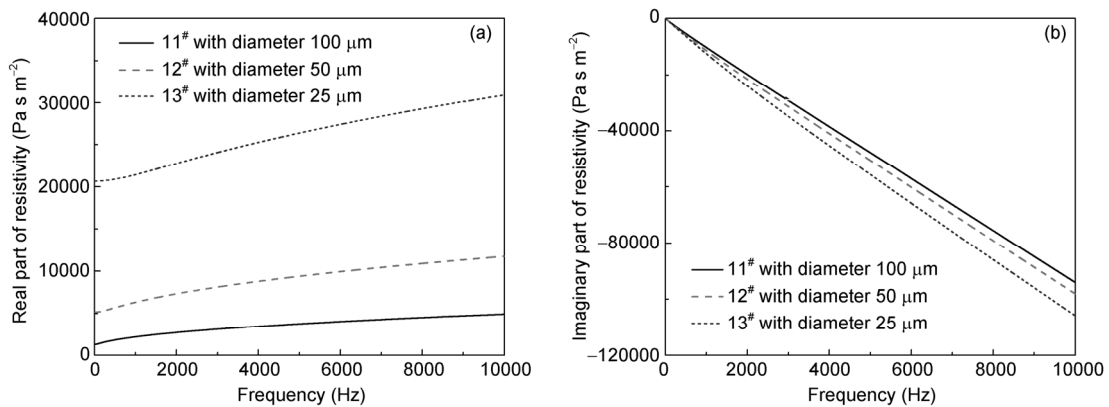

Figure 9   Influence of fiber diameter on flow resistivity of single-layer fibrous metal (samples 11#, 12# and 13#). (a) The real part of flow resistivity; (b) the imaginary part of flow resistivity.
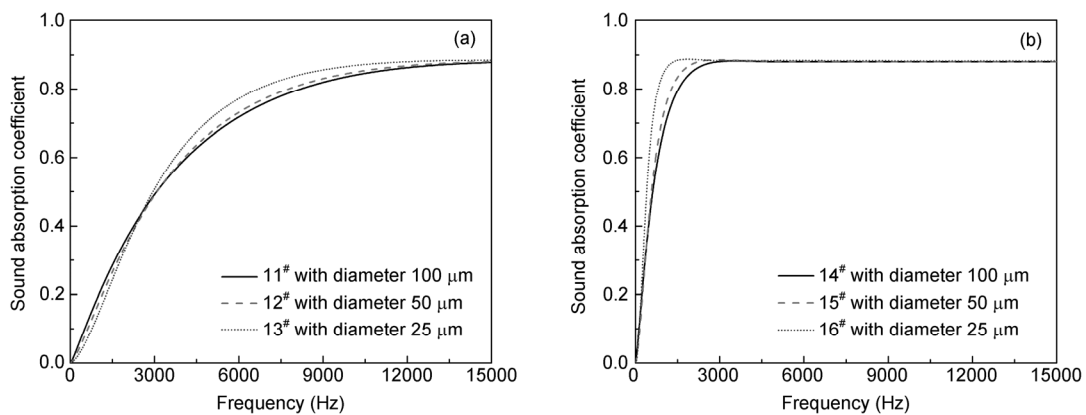

Figure 10   Influence of fiber diameter on sound absorption coefficient of single-layer fibrous metal with thickness: (a) 10 mm (samples 11[#], 12[#] and 13[#]); (b) 50 mm (samples 14[#], 15[#] and 16[#]). Porosity fixed at 0.95; no air cavity between sample and rigid wall.

the sample thickness is increased, comparison between Figures 10(a) and (b) reveals that sound absorption resonance is shifted to lower frequency. Consequently, the sound absorption coefficient reaches its maximum stable value earlier. Nonetheless, the maximum stable value is almost independent of fiber diameter, indicating that the amount of sound entering the fibrous material is dictated by porosity as shown in the previous section.

4.3 Influence of air gap

Figure 11 plots the sound absorption coefficient of single layer sample 17 (Table 3) as a function of frequency for air gap thicknesses. As can be seen from Figure 11, the air gap has a great influence on the sound absorption of the fibrous material. As the thickness of the air gap is increased, the peaks and valleys of the curve is increasingly shifted to the left (Figure 11) and hence the sound absorption coefficient increases significantly in the low frequency range. As is known, if the distance between the incident and reflected sound is the odd number times of 1/4 wavelength, a peak appears in the sound absorption coefficient curve. In contrast, if the distance is multiples of the 1/2 wavelength, a dip shows up in the curve. The presence of the air gap enlarges the distance between the incident and reflected waves, so the peaks and valleys all move to lower frequencies accordingly. In the high frequency range (>4000 Hz for the case considered in Figure 11), the sound absorption does not change with varying thickness of the air gap since the sound energy dissipated by the air can be ignored here.

5 Influence of physical parameters: Multi-layer fibrous metal

In this section, we aim to investigate how sound absorption changes with the variation of physical parameters and obtain basic principles for the design of multi-layer fibrous sam-
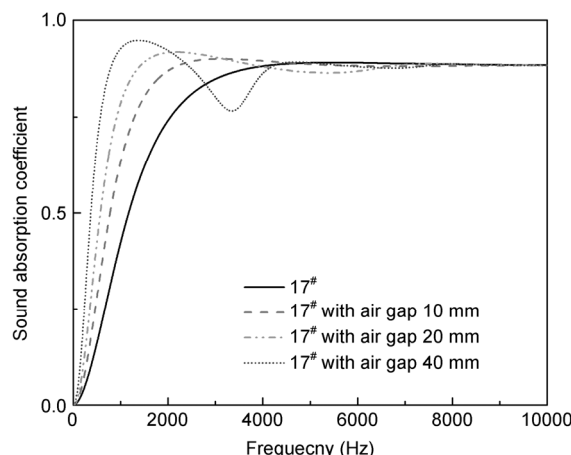

Figure 11 Influence of air gap thickness on sound absorption coefficient of single-layer fibrous metal with thickness 20 mm, porosity 0.95 and fiber diameter 20 μm (sample 17#).

ples. We use multi-layer samples with 2 different fibrous layers of 10 mm thickness each as examples for simplicity. In Figure 12, the predicted sound absorption coefficient of multi-layer samples with either decreasing or increasing physical parameters (porosity and fiber diameter) as listed in Table 4 is compared with uniform (single-layer) samples having the same averaged physical parameters.

It can be seen from Figure 12(a) that the porosity variation has a significant effect on the sound absorption coefficient of the sintered fibrous materials. In comparison to the uniform sample, the sound absorption coefficient of a multi-layer sample with increasing porosity is larger in the low frequency range while smaller in the high frequency range. Conversely, the sound absorption of a sample with decreasing porosity is smaller at low frequencies while larger at high frequencies than its uniform counterpart. This phenomenon may be attributed to the change of the characteristic impedance ratio ($\gamma = \rho c / \rho_0 c_0$) between the fibrous material and air, which is induced by the porosity variation distribution in the fibrous material. The sample with increasing porosity
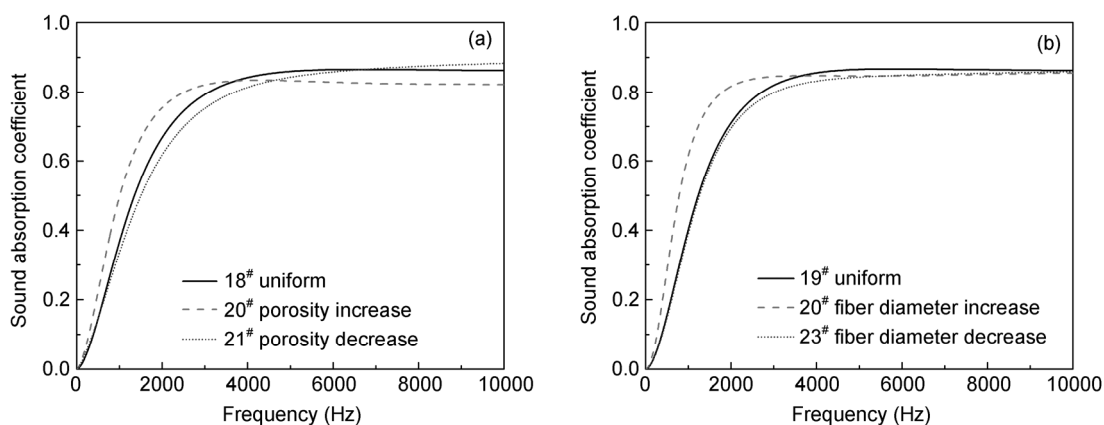

Figure 12 Sound absorption coefficient of multi-layer fibrous metal composed of 2 uniform layers. (a) Influence of porosity gradient (samples 20# and 21#); (b) influence of fiber diameter gradient (samples 22# and 23#).

Table 4   Multi-layer fibrous metal samples used for parameter study

Sample number	Fiber diameter (μm)		Porosity (%)		Thickness (mm)	
	First layer	Second layer	First layer	Second layer	First layer	Second layer
20	50	50	82	98	10	10
21	50	50	98	82	10	10
22	20	60	90	90	10	10
23	60	20	90	90	10	10

has a higher γ value while the one with decreasing porosity has a lower value than that of the uniform sample. It is worth mentioning that, as the characteristic impedance ratio is increased, the sound absorption resonance shifts to lower frequency, causing the trends of the sound absorption curves shown in Figure 12(a).

From Figure 12(b) it can be seen that the variation of fiber diameter also has significant effect on the sound absorption of multi-layer fibrous metal, especially in the low frequency range. Relative to a uniform sample, sample 22 with increasing fiber diameter absorbs considerably more sound in the low frequency range and little less sound in the high frequency range. In contrast, the sound absorption ability of sample 23 with decreasing fiber diameter drops slightly over the whole frequency range compared with the uniform sample. Again, the variation trends of the sound absorption curves shown in Figure 12(b) are closely related to the alteration of the characteristic impedance ratio between fibrous material and air, which changes as the fiber diameter variation is varied.

6   Conclusions

A theoretical model is developed on the basis of dynamic flow resistivity to investigate the sound absorption performance of single- and multi-layer sintered fibrous metal, which is only dependent on two basic parameters, namely, fiber diameter and porosity. The fibrous metal is modeled as randomly distributed parallel fibers so that the dynamic flow resistivity can be favorably estimated using the existing results for simplified stack of fibers. Upon calculating the sound propagation constant and characteristic impedance by using the estimated flow resistivity, the sound absorption coefficient of the fibrous material is determined by employing an empirical model. Subsequently, the sound absorption coefficient of multi-layer fibrous metal is calculated via recursion formulas for surface impedance. The validity of the model predictions is checked against experimental measurements for both single- and multi-layer sintered fibrous metal samples, with good agreement achieved. Finally, the model is employed to quantify the effects of key physical parameters on sound absorption of the sintered fibrous materials. The following conclusions are drawn.

For uniform (single-layer) samples, as the porosity affecting the amount of sound entering the fibrous material is reduced, the sound absorption coefficient increases in the low frequency range while decreases in the high frequency range.

For uniform (single-layer) samples, the sound absorption coefficient increases with decreasing fiber diameter in the high frequency range, due mainly to the increase of flow resistivity. In contrast, in the low frequency range, the sound absorption ability of the fibrous material decreases with decreasing fiber diameter, as the sound energy is mainly dissipated by the damping effect of fiber vibration itself rather than the viscous effect between the air and fiber.

Since the backed air gap acts to enlarge the thickness of the fibrous material, the sound absorption resonance and anti-resonance are shifted to lower frequencies. Accordingly, in the low frequency range, the sound absorption coefficient increases as the air gap thickness is increased.

For multi-layer samples, increasing the porosity variation helps to improve sound absorption in the low frequency range but leads to inferior sound absorption in the high frequency range. Decreasing the porosity variation has an opposite effect.

Increasing the variation of fiber diameter enhances sound absorption only at the low frequency. In contrast, reducing the variation of fiber diameter causes inferior sound absorption over the whole frequency range.

1   Tang H, Zhu J, Ge Y, et al. Sound absorbing characteristics of fibrous porous materials gradient structure. Rare Metal Mat Engin, 2007, 36: 2220–2223

2   Zhang B, Chen T. Calculation of sound absorption characteristics of porous sintered fiber metal. Appl Acoust, 2009, 70: 337–346

3   Sun F, Chen H, Wu J, et al. Sound absorbing characteristics of fibrous metal materials at high temperatures. Appl Acoust, 2010, 71: 221–235

4   Zwikker C, Kosten C W. Sound Absorbing Materials. New York: Elsevier, 1949. 26–34

5   Biot M A. Theory of propagation of elastic waves in a fluid-saturated porous solid. I. Low-frequency range. J Acoust Soc Am, 1956, 28:

168–178

6 Biot M A. Theory of propagation of elastic waves in a fluid-saturated porous solid. II. Higher frequency range. J Acoust Soc Am, 1956, 28: 179–191

7 Attenborough K. Acoustical characteristics of rigid fibrous absorbents and granular materials. J Acoust Soc Am, 1983, 73: 785–799

8 Johnson D L, Koplik J, Dashen R. Theory of dynamic permeability and tortuosity in fluid-saturated porous-media. J Fluid Mech, 1987, 176: 379–402

9 Champoux Y, Allard J F. Dynamic tortuosity and bulk modulus in air-saturated porous-media. J Appl Phys, 1991, 70: 1975–1979

10 Wilson D K. Relaxation-matched modeling of propagation through porous media, including fractal pore structure. J Acoust Soc Am, 1993, 94: 1136–1145

11 Champoux Y, Stinson M R. On acoustical models for sound propagation in rigid frame porous materials and the influence of shape factors. J Acoust Soc Am, 1992, 92: 1120–1131

12 Narang P. Material parameter selection in polyester fibre insulation for sound transmission and absorption. Appl Acoust, 1995, 45: 335–358

13 Voronina N. Acoustic properties of fibrous materials. Appl Acoust, 1994, 42: 165–174

14 Voronina N. An empirical model for rigid frame porous materials with high porosity. Appl Acoust, 1997, 51: 181–198

15 Voronina N. An empirical model for elastic porous materials. Appl Acoust, 1998, 55: 67–83

16 Voronina N. An empirical model for rigid-frame porous materials with low porosity. Appl Acoust, 1999, 58: 295–304

17 Voronina N, Horoshenkov K. A new empirical model for the acoustic properties of loose granular media. Appl Acoust, 2003, 64: 415–432

18 Garai M, Pompoli F. A simple empirical model of polyester fibre materials for acoustical applications. Appl Acoust, 2005, 66: 1383–1398

19 Delany M E, Bazley E N. Acoustical properties of fibrous absorbent materials. Appl Acoust, 1970, 3: 105–116

20 Miki Y. Acoustical properties of porous materials–Modifications of Delany-Bazley models. J Acoust Soc Jap (E), 1990, 11: 19–24

21 Allard J F, Champoux Y. New empirical equations for sound propagation in rigid frame fibrous materials. J Acoust Soc Am, 1992, 91: 3346–3353

22 Komatsu T. Improvement of the Delany-Bazley and Miki models for fibrous sound-absorbing materials. Acoust Sci Tech, 2008, 29: 121–129

23 Tang H, Zhu J, Wang J, et al. Sound Absorption Characters of Metal Fibrous Porous Material. Montreal: DEStech Publications, Inc, 2007. 181

24 Huang K, Yang D H, He S Y, et al. Acoustic absorption properties of open-cell Al alloy foams with graded pore size. J Phys D: Appl Phys, 2011, 44: 365405

25 Dupère I D J, Lu T J, Dowling A P, et al. Microstrutural optimization of celluar acoustic materials. J Xi'an Jiaotong Univ, 2007, 41: 1251–1256

26 Tarnow V. Calculation of the dynamic air flow resistivity of fiber materials. J Acoust Soc Am, 1997, 102: 1680–1688

27 Sangani A S, Yao C. Transport processes in random arrays of cylinders. II. Viscous flow. Phys Fluid, 1988, 31: 2435–2444